

# Scalings of axisymmetric granular column collapse

J. M. Warnett · P. Denissenko · P. J. Thomas ·  
E. Kiraci · M. A. Williams

Received: 4 March 2013 / Published online: 7 December 2013  
© Springer-Verlag Berlin Heidelberg 2013

**Abstract** Experimental investigations into the collapse of granular columns are presented with dimensional results of the final deposit obtained using a 3D laser scanner. The high accuracy measurement method has found that the final pile radius is not only dependent on the aspect ratio of the initial geometry as previously thought, but also the initial column radius and hence the ratio of column radius to particle diameter. This was also observed to be true for the angle at the base of the deposit. Theoretical considerations coupled with obtained data have allowed the angle at summit for aspect ratios less than approximately 3 to be described entirely in terms of material parameters and aspect ratio—something desired for all length scalings but seemingly unobtainable due to the dynamic nature of the collapse. With the method being non intrusive, measurement of the summital radius was also made possible. The final height showed a dependence predominantly with aspect ratio in agreement with previous authors.

**Keywords** Granular collapse · Granular flow · Failure surface · Avalanches

## 1 Introduction

Granular flows have been the interest of much research due to their existence in many man made processes and natural

phenomena. The handling of grains and powders is important to many civil engineering projects, such as the storage of grains and powders, and also to the pharmaceutical industry in the sorting of pills and medicines. Description of these flows have been offered by interpretation of the collapse of a granular column [1–8] and the failure of a granular step [9–11]. The avalanching flows observed in these experiments are analogous to some geophysical flows. Examples such as pyroclastic flows and avalanches are of particular interest for hazard management, but direct observation of these flows are rare and dangerous to undertake. Predictions of such deluges are based on the final deposits [12] and so the dynamics of collapse can be difficult to describe over specific geographic topologies with variability in the landscape.

The collapse of an axisymmetric granular column is an unsteady flow; there are phases of acceleration, steady flow and deceleration during the collapse. This dynamic is further complicated by the existence of static and flowing regions within the collapsing column. A general physical description of avalanching granular flows is given by Cates et al. [13] in terms of mechanisms behind the development of a sand pile. A sand pile can be seen as ‘fragile’ in that it cannot elastically support some infinitesimal loads. This fragility leads to avalanching and settles where grains have successfully jammed under the load of a granular force chain. A slight change in the direction of the force acting on a grain at the extremity (surface of the pile) can break this chain and results in further reorganisation of the previously jammed medium below and additional avalanching.

Theoretical models of granular flows have been developed using depth-averaged and Saint–Venant equations, applied with a varying degree of success dependent upon the flow regime [14–17]. This is due to the lack of a set of constitutive laws as in fluidic systems. The collapse of a granular column is a highly unsteady example of a granular flow and

---

J. M. Warnett (✉) · P. Denissenko · P. J. Thomas  
School of Engineering, University of Warwick, Gibbet Hill Road,  
Coventry CV4 7AL, UK  
e-mail: j.m.warnett@warwick.ac.uk

E. Kiraci · M. A. Williams  
Warwick Manufacturing Group, University of Warwick,  
Gibbet Hill Road, Coventry CV4 7AL, UK

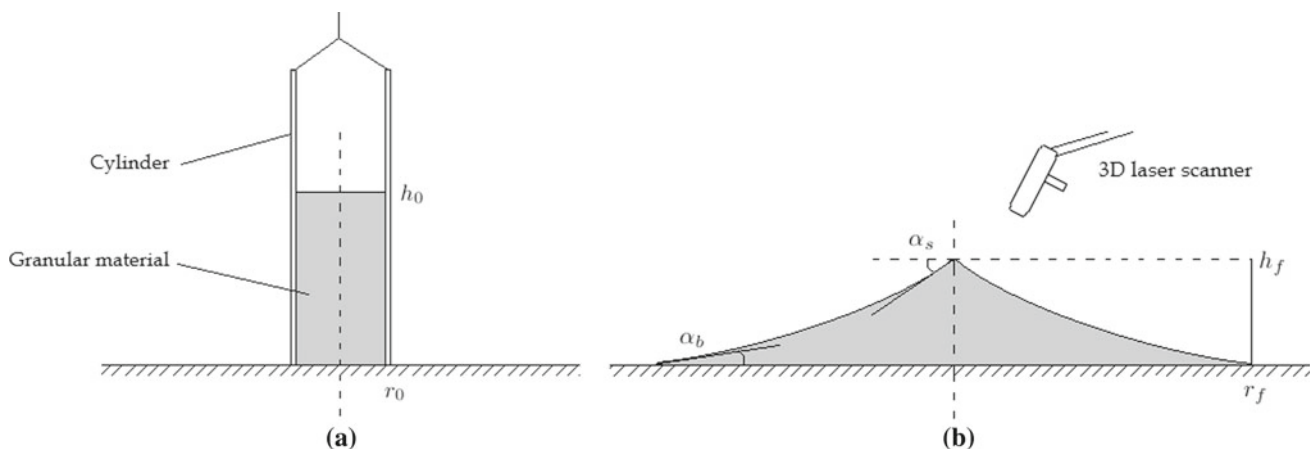


**Fig. 1** Experimental setup. **a** Initial setup of granular column on rotating table. **b** Column after collapse with dimensions

applying these sets of equations struggled to recover the precise dynamic behaviour of the system [18]. Much progress has been made in this area with a different combination of models; for example Larrieu et al. [19] used a combination of shallow water depth-averaged equations with the regular timed addition of material to the flow. This model is in good agreement with the scalings already found experimentally up to an aspect ratio of  $a < 10$ , but requires an unphysical friction coefficient. This is in addition to the evolution of the profile of the deposit often being exaggerated. Even greater progress has been made in the collapses' 2D counterpart, the failure of a granular step. This particular collapse while largely exhibiting similar flow regimes results in slightly different scalings, suggested to be due to the geometry dependent mechanism of side-ways mass ejection [4]. Doyle et al. [20] adapted the model proposed by Larrieu et al. by including an estimation for the interface between the static and flowing region which allow a more realistic coefficient of friction. Crosta et al. [21] used a Mohr–Coulomb yield rule with non associative flow that was in very good agreement with the physical experiments, although struggled with the tapering of the front of the flow. The most encouraging and accurate model to date, again in 2D, is the  $\mu(I)$  rheology proposed by Lagree et al. [22] recovering the evolution of the flow with a greater accuracy. In the future it is hoped that the  $\mu(I)$  rheology can be successfully applied to the 3D cylindrical column collapse case.

Computationally this collapse has been investigated by discrete-element modelling (DEM) simulations; in 2D by Staron and Hinch [4] and Zenit [5], and in 3D by Cleary and Frank [6]. Knowing that scalings achieved for the 2D collapse [9–11] display variations from its axisymmetric counterpart, comparison is best drawn from the 3D case. Cleary and Frank demonstrate that particle shape is a limiting factor in reproducing experimental results and achieve values obtained by both Lube et al. [1] and Lajeunesse et al. [2] for their singular test case. Non spherical particle models, particularly in 3D,

consume a much larger amount of computational power and reasons why this investigation has not been taken further.

Several previous authors [1–3] have investigated the collapse of an axisymmetric column and have concluded several simple scaling laws based on the initial aspect ratio of the granular column. Lube et al. [1] used a vernier scale and laser pointer technique with a stated accuracy of  $\pm 0.1$  mm to dimensionalise the final column, where as Lajeunesse et al. [2] used a camera imaging technique with a spatial resolution of 0.4 mm. In this study a different experimental technique is applied where a 3D laser scanner with a substantially higher accuracy of  $\pm 0.04$  mm is employed for data acquisition with the added benefit of digitizing the result for analysis and further interrogation. Experiments performed using this technique with similar initial system sizes to those of previous authors have revealed a variation of previously proposed dimensional scalings with a dependence on this initial system size. The experimental method has also allowed investigation into the angular profile of the deposit and the rate at which the summit is consumed with an increase in aspect ratio.

## 2 Experimental setup

### 2.1 Apparatus

The apparatus was set up as in Fig. 1. A cylinder of radius  $r_0$  was placed on a smooth perspex plane and partially filled with granular media of mass  $m_0$  to a specified height  $h_0$ . The aspect ratio,  $a = h_0/r_0$ , was varied for a single cylinder radius  $r_0$  by varying the mass of the particulate,  $m_0$ . A number of cylinder radii were used with a range of aspect ratios as outlined in Table 1. The experiments were performed in a randomised order to prevent systematic errors from affecting the final results.

In these experiments the granular media used was a limestone particulate with bulk density  $\rho = 1.5$  g/cm<sup>3</sup> and a

**Table 1** Range of aspect ratios  $a$  trialled for each cylinder of radius  $r_0$  and associated  $r_0/d$  value

$r_0$ (mm)	$r_0/d$	$a$ range
20	28	0.24–8.69
25	35	0.30–7.00
30	42	0.20–6.05
35	50	0.24–5.29
40	57	0.25–4.40
45	64	0.24–4.02
75	107	0.28–1.69

dynamic angle of repose of  $\theta_r \approx 30^\circ$ . The angle of repose is the maximal angle to the horizontal sustained by a pile of granular material before the slope face begins to slide. This value was given by the manufacturer and was confirmed experimentally by slowly funneling the particulate onto a horizontal surface and finding the greatest slope of the resulting deposit.

To ensure repeatable initial conditions grains were sieved prior to filling to select grains of diameter  $d = 0.6 - 0.8$  mm, which were then funneled into the cylinder and the top gently flattened. This results in a non-dimensional system size parameter defined as  $r_0/d$ . The mean packing density of the material in the cylinder is calculated  $\phi = m_0/(\rho\pi r_0^2 h_0)$ , and found to be 0.78–0.82.

The cylinder was connected to rope over a series of pulleys that was mounted above the table. The cylinder was removed quickly by pulling on the rope at a speed greater than the speed of collapse to ensure minimal interference with the collapse itself. An average speed of  $1.8 \text{ ms}^{-1}$  was found to be sufficient. After release, the material spreads across the table resulting in a final deposit.

A 3D scanner was then used to digitize the resulting deposit enabling precise dimensionalisation of the pile by use of the analysis software ‘*Geomagic Qualify*’ (3D Digital 2002; Geomagic, Research Triangle Park, NC, USA). This enabled non-contact measurement with high accuracy and a greater amount of interrogation in comparison to previous studies.

## 2.2 Data capture and scanner calibration

The 3D laser scanner used in this study was the ‘*Nikon Metrology MCA 2400 M7*’ articulated arm enabling complete detailed geometric scans of the sand piles. The scanner head produced a laser stripe that was made to traverse the deposit, capturing data points viewable in real time providing immediate feedback on the scanning pace, progress and scanned area. The scanner was able to scan areas as large as  $470 \text{ mm} \times 470 \text{ mm}$  which was a limitation in terms of allowable aspect ratio ranges shown in Table 1.

A typical scan path consisted of 1,000 measurement points per stripe. To maintain a consistent number of measurement points per scan path and reduce the level of data noise it is critical to sustain the optimum distance between the scanning head and deposit. The scanner produced a laser guide with the stripe enabling the laser user to maintain this distance and obtain quality data. With this level of precision, the obtained point cloud contained 800–900 points per  $\text{cm}^2$ . When using the equipment to scan objects with defined edges, numerous scans can be easily amalgamated to produce the final object. The software was found to struggle performing this task with granular heaps due to the largely uneven surface and so all scans were completed in a single motion of the articulated arm.

The laser intensity also has an impact on the quality of data achieved, and this is managed by the equipment itself to include adjustments according to lighting conditions. Once the system is fully calibrated the lighting levels were maintained and temperature controlled at  $\pm 5^\circ\text{C}$  relative to the temperature when calibrated. Single point and length accuracy of the scanner is 31 microns and 42 microns  $\pm 2\sigma$  respectively. These values were determined by point repeatability and volumetric accuracy tests as outlined in the industrial standard ASME B89.4.22 [23,24].

## 2.3 Processing and accuracy

The point cloud generated was interpreted as a surface mesh as in Fig. 2 using ‘*Geomagic Qualify*’; industrial standard software used for the inspection of scanned objects and materials. On occasion particles can be ejected a measurable distance further from the edge of the resultant pile. These were easily identifiable and removed from the final mesh for evaluation.

The global coordinate system of the mesh was altered so the table that the deposit rested on aligned with the x-y plane. Four 2D cross sections were taken of the resultant mesh through the centre of the pile. The ability to take several 2D cross sections of the final deposit allowed evaluation of the initial setup and cylinder removal. The cross sections made it easy to find where the cylinder had not been raised vertically as the resultant pile would be asymmetric, so adjustments could be made to the equipment in trials before the main experiments were run.

The achieved cross sections were then used to retrieve several dimensions of the final deposit indicated in Fig. 1; the final pile radius,  $r_f$ , the final pile height,  $h_f$ , the summital angle,  $\alpha_s$ , the angle at the base,  $\alpha_b$ , and in the case of a truncated cone,  $r_s$ , the summit radius. In the case of all these measurements with the exception of the final pile height, an average was taken across all four 2D cross sections where there is known to be variability due to an uneven periphery.

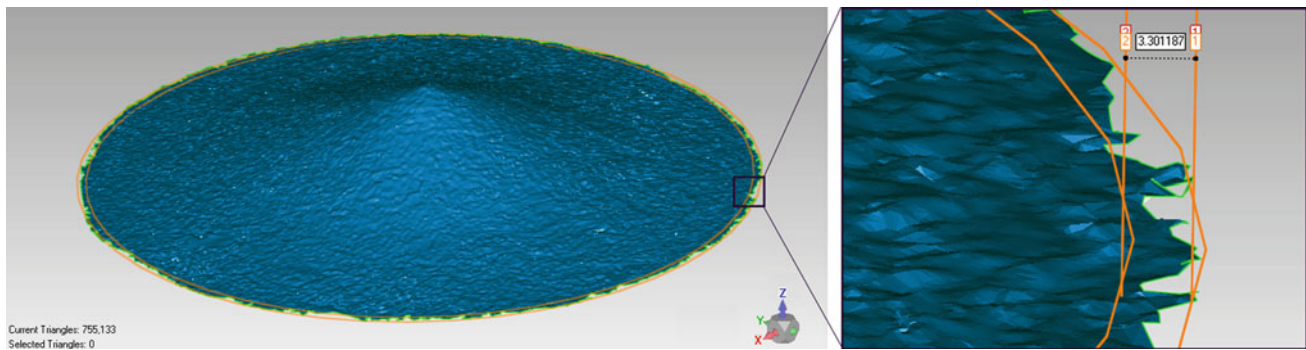


**Fig. 2** Example surface mesh for  $r_0 = 45$  mm  $a = 1.87$  produced from point cloud achieved with laser scanning of the resultant deposit. Boundary effect demonstrated by two orange periphery lines formed

from the inner most and outer most points. The distance between these boundaries is 3.30 mm, approximately  $4.7d$

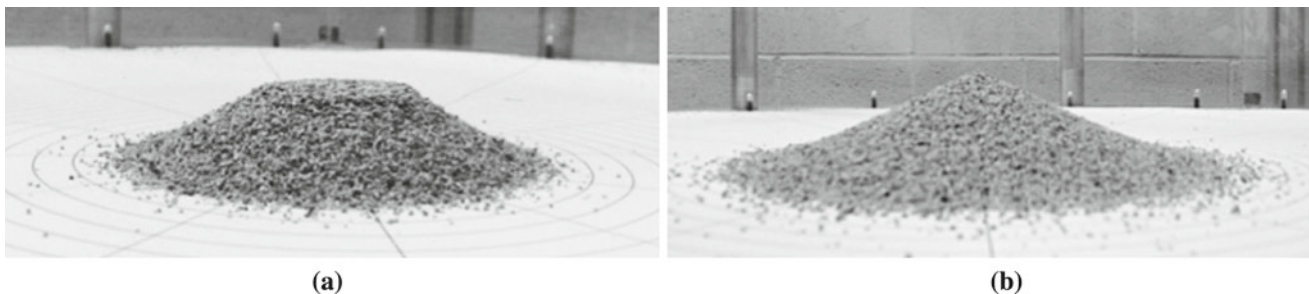


**Fig. 3** Two distinct morphologies arise dependent upon aspect ratio  $a$ . **a** Truncated cone when  $a < 0.90$ . **b** Sloping conical shape when  $a > 0.90$

Repeatability testing was performed on several initial aspect ratios and cylinder sizes to determine the maximal variation in dimensional quantities. The largest source of error within a single collapse can be observed at the periphery of the pile where grains do not fall into a clearly defined edge. Figure 2 highlights the smallest and largest possible boundaries in a particular example while displaying the deviation from the possible edges. Across varying aspect ratios this was observed to be  $3d$  ( $\pm 1.1$  mm) where  $a < 0.50$  up to  $5d$  ( $\pm 1.8$  mm) for  $a > 2$ , confirmed by inspection of the resultant scans. Averaging across the four 2D cross sections in this way finds the mean periphery profile of the deposit. Results from the repeatability testing and accounting for the error due to the uneven rim of the deposit, dimensional quantities were found to vary as  $r_f = \pm 1.6 - 2.3$  mm (aspect ratio dependent),  $r_s = \pm 2.0$  mm,  $h_f = \pm 0.5$  mm, and angular quantities  $\pm 1^\circ$ . The material was measured to within  $\pm 0.1$  g, allowing only a variability in packing.

### 3 Experimental observations

#### 3.1 Flow description and morphology

Qualitative descriptions of the collapse have been previously studied by other authors [1,2]. For  $a \lesssim 3$  the periphery of the column crumbles vertically downwards resulting in a frontal

flow to develop at the foot of the column that propagates radially outwards. Subsequently collapsing layers flow over the surface of the deposit continuing the flow in the radial direction. This results in a secondary front which separates the frontal flow and the currently static summittal region, which propagates inwards. This results in a circular discontinuity between the two regions, which is eventually consumed by the avalanche and the flow continues until stability is achieved in the summittal region of the deposit.

In this range two distinct morphological deposits that can be seen in Fig. 3. For shallow columns where  $a < 0.90$  the summit is never completely consumed by the avalanche and results in a truncated cone. Upon exceeding this aspect ratio the summit is entirely consumed and a full conical shape is left. Previous authors have found this critical aspect ratio to be  $a = 0.74$  [1,2]. Without direct inspection with a 3D scanner, it can be difficult to determine where one geometric regime ends and the second begins as a summit may still exist but is small. It is for these reasons that a higher value is expected to be achieved, although this maybe compounded with the difference in granular material.

With the non-intrusive accurate measurement capabilities the rate of consumption of the summittal plateau was also observed. The variation of the summit radius,  $r_s$ , with aspect ratio is shown in Fig. 4 where  $r_s$  is normalised against the initial radius as

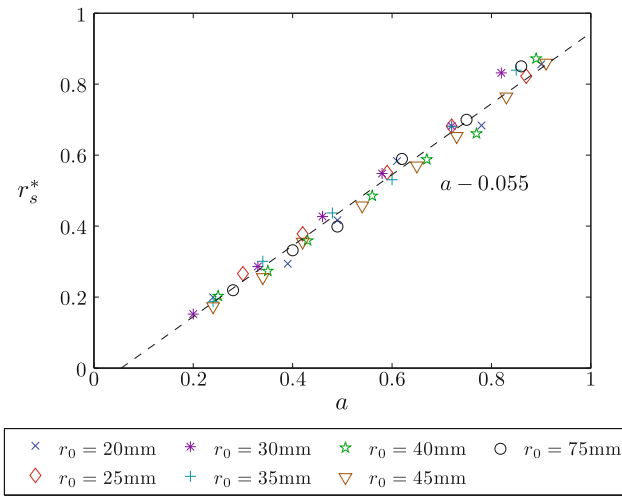


**Fig. 4** Variation of normalised summital radius  $r_s^* = (r_0 - r_s)/r_0$  against aspect ratio. Dashed line indicates linear fit given in Eq. (2)

$$r_s^* = \frac{r_0 - r_s}{r_0} \tag{1}$$

This shows a common linear relation across all cylinder sizes given by

$$r_s^* = a - 0.055 \tag{2}$$

valid for  $a < 0.90$ . Where  $a > 0.90$  there is a sharp deceleration in the shrinking of the plateau with increasing aspect ratio as the peak becomes curved and the summital plateau becomes indistinguishable as it is of the order of a few grain sizes.

The direct proportionality observed is expected with consideration of geometric arguments. Under the first regime, the collapse results in a truncated cone. Hence

$$r_s = r_0 - h_0 \tan \bar{\theta} \tag{3}$$

for some mean angular profile of the slope of the deposit  $\bar{\theta}$ . Some rearrangement gives

$$r_s^* = a \tan \bar{\theta} \tag{4}$$

in agreement with the obtained data.

Where  $a \gtrsim 3$  the collapse dynamic changes from that previously observed. In this case the whole upper surface of the column moves, initially retaining its horizontal profile. A frontal flow then develops at the base on the pile as before spreading radially outwards. Part way through the collapse the upper surface begins to dome while the frontal flow continues to spread. The end result is a deposit with a shallower angular profile than lower aspect ratios.

The evolution of the profile with increasing aspect ratio can be seen in Fig. 5a for  $r_0 = 35$  mm. The height,  $h(r)$  is given as a function of radius,  $r$ , and both values are normalised against  $r_0$ . It is evident that the angular profile not only becomes shallower with increasing  $a$ , but the nose of the deposit becomes less sharp and displays an increase in curvature. The relationship between defining dimensional values and aspect ratio are discussed in detail below to include the final deposit radius,  $r_f$ , final height,  $h_f$ , and angles at the summit,  $\alpha_s$ , and base,  $\alpha_b$ . This has previously been investigated by Lube et al. [1] and Lajeunesse et al. [2] but a further dependence has emerged; a dependence on the initial system size  $r_0/d$ .

Similar system sizes were used as in previous experimental works, but notable differences in the defining dimensional values were found and are presented in this study. An example of resultant deposit profiles for  $a = 1.7$  is given in Fig. 5b for several cylinder sizes. In this particular case the final height and angle at the summit is largely the same. The difference occurs at the nose of the deposit where larger system sizes result in a greater final deposit radius and a shallower angle

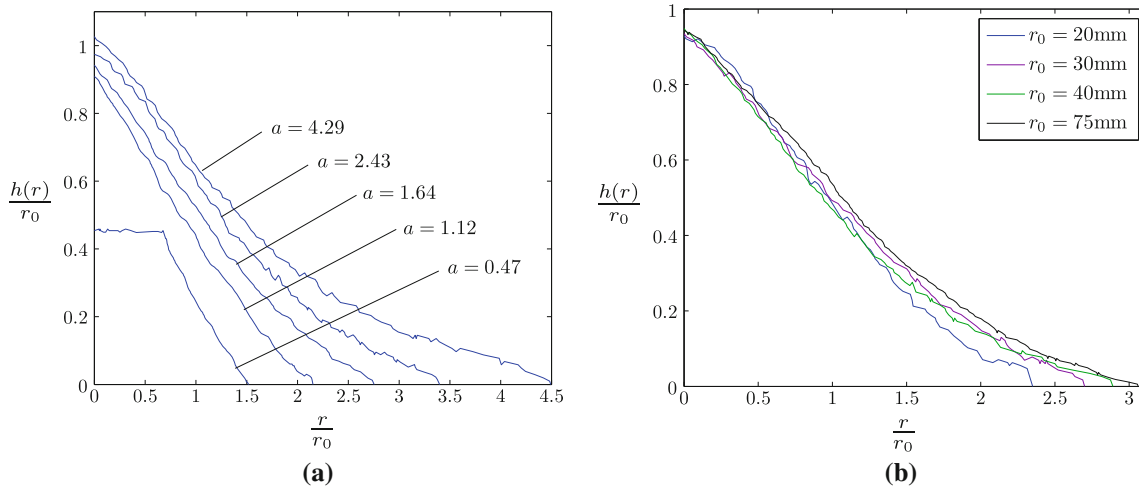


**Fig. 5** Deposit profiles normalised against the cylinder radius  $r_0$ . **a** Evolution of the profile with increasing aspect ratio  $a$  for  $r_0 = 35$  mm. **b** Difference in profiles for  $a = 1.70$

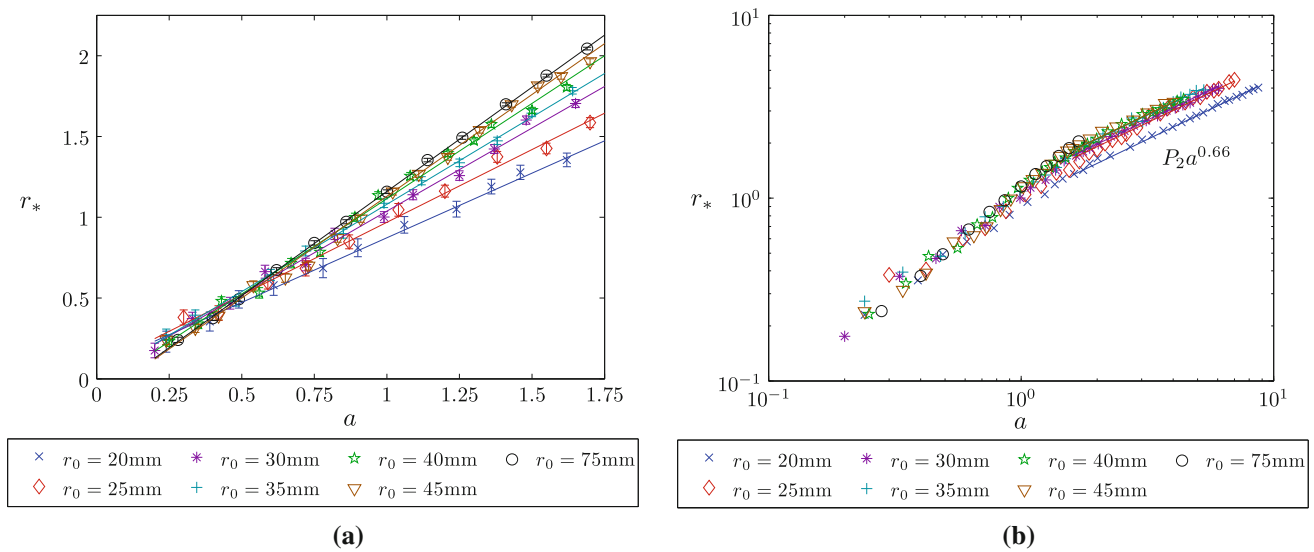


**Fig. 6** Relationship between  $r_*$  and  $a$  for varying cylinder radii  $r_0$  with coefficients given in Table 2. **a**  $a < 1.7$  with errors displayed as discussed in Sect. 2.3. Linear fits for each  $r_0$  satisfying Eq. (6) are shown. **b**  $a \gtrsim 1.7$  following a power law relation as indicated by line fit

at the base. The impact of  $r_0/d$  is considered for each of the dimensional quantities and frequently displays an arresting value of this effect. Meso-scale interactions are known to occur across granular systems but in this case it has been previously overlooked.

### 3.2 Final pile radius

Previous results [1–3] suggested that the final deposit radius is independent of the initial system size. Final pile radius,  $r_f$ , against aspect ratio was considered for each cylinder radius, with  $r_f$  normalised against  $r_0$  as

$$r_* = \frac{r_f - r_0}{r_0} \tag{5}$$

#### 3.2.1 Low aspect ratios

First consider where  $a < 1.7$  as shown in Fig. 6. A linear relation of the form

$$r_* = P_1 a + Q \tag{6}$$

where  $P_1$  and  $Q$  are constants is observed, but there is a clear dependence of these coefficients on the initial cylinder size and inherently the system size. The gradient  $P_1$  for each cylinder radii is given in Table 2. It evidently increases with cylinder radii although it indicates strong signs of arresting. For  $r_0 = 20 - 45$  mm it follows a strongly linear relation given by:

$$P_1 = 0.013 \frac{r_0}{d} + 0.45 \tag{7}$$

**Table 2** Variation in proportional constants  $P_1$  and  $P_2$  for relationship between  $r_*$  and  $a$  given by Eqs. (6) and (9) and respectively

$r_0$ (mm)	$r_0/d$	$P_1$	$P_2$
20	28	0.79	1.00
25	35	0.88	1.21
30	42	1.02	1.25
35	50	1.06	1.33
40	57	1.18	1.34
45	64	1.26	1.34
75	107	1.29	–

and substituting this into Eq. 6 gives

$$r_* = 0.013 \frac{h_0}{d} + 0.45a + Q \tag{8}$$

This reveals a secondary dependence on initial height  $h_0$  while the system size  $r_0/d \lesssim 70$ . The increase in  $P_1$  severely slows for the largest cylinder size and while limitations of the equipment prevent investigation of larger values of  $r_0/d$ , it is presupposed that this deceleration continues in strength with increases in  $P_1$  being negligible. This disputes previous research by other authors [1–3] who conclude there is no such effect while investigating comparable values of  $r_0/d$ , although it is worth noting that the gradient for  $r_0 = 75$  mm,  $P_1 = 1.29$ , is close to the value of 1.24 achieved by Lube et al. With previous experiments subject to greater inaccuracies in their measurement methods, differences in achieved data have previously been assumed to be due to experimental error. The high spatial resolution in the presented results and strong variation in  $P_1$  indicates the existence of this dependence to be correct. Reasoning for this

difference in scaling can be given insight by consideration of the degree of mass flow and process of jamming and flowing layers as described by Cates et al. [13].

Consider a fixed aspect ratio  $a = h_0/r_0$  for two different initial column radii  $r_0$  with  $r_0/d < 70$ . The larger  $r_0$  will initially contain more granular matter and so at the start of the avalanche, the larger  $r_0/d$  will have a greater initial deposit on the surface. The larger initial deposit has a greater amount of jammed grains under a larger amount of pressure and hence a longer granular force chain length. In both cases the subsequently avalanching layers will disturb the force chain but a smaller proportion of the force chain will be disturbed in the case of the larger deposit due to the stronger jamming effect and the grains being under a greater amount of pressure. This results in a smaller proportion of the flowing layer being entrained in the disturbed surface and hence a smaller proportional energy loss in the flowing layer. This allows for greater movement of the avalanching layer and overall a greater runout. Where we observe a saturation of the meso-scale effect and considering two different values of  $r_0/d$ , the proportion of the force chain that will be disturbed in the collapse will be small and comparable to other larger values of  $r_0/d$ . For this reason it is reasonable to expect to observe the arresting effect seen in the proportional constant  $P_1$  of the final pile radius relation.

### 3.2.2 Larger aspect ratios

When  $a \gtrsim 1.7$  a new relation begins to emerge with a good fit to a the power law

$$r_* = P_2 a^{0.66} \tag{9}$$

where  $P_2$  varies for  $r_0/d$  as given in Table 2. Compared to the relation given in Eq. (6) this constant appears to arrest earlier having stagnated when  $r_0 = 35$  mm,  $r_0/d = 50$ . The difference in  $P_2$  can be attributed to the earlier discussion on jamming with its quicker cessation likely to be due to the greater amount of material involved in the collapse. The data is in agreement with Lube et al. in terms of the onset of Eq. (9), but the power 0.66 is higher than both Lube et al. and Lajeunesse et al. who agree with a square root fit. The variation in the precise value of the power could be due to different granular materials used to the other authors, but again they negate the effect of  $r_0/d$  as the data clearly shows.

### 3.3 Final height

The final height was normalised as  $h_* = h_f/r_0$  and compared against  $a$  in Fig. 7. In the first geometric regime where  $a < 0.90$  the deposit is a truncated cone and so  $h_f = h_0$ . This suggests that there is an internal conical surface over which the avalanche occurs, with the angle at the base of this internal cone to be  $\theta = \tan^{-1}(0.90) = 42.0^\circ$ . This obser-

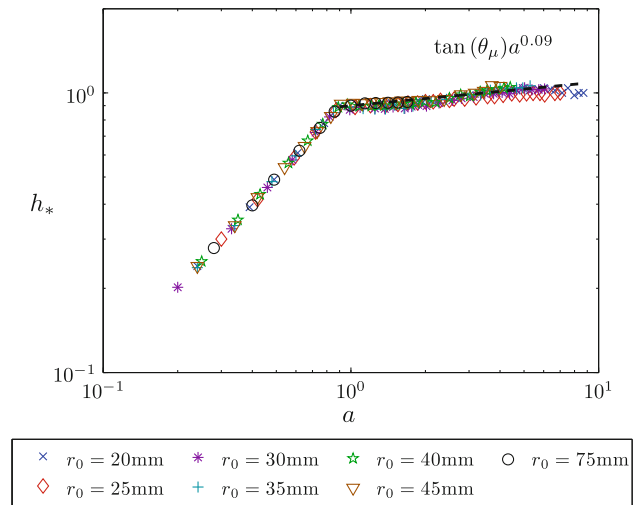


**Fig. 7** Evolution of normalised height  $h_*$  with aspect ratio  $a$ . Dashed line indicates power law relation given by Eq. (10)

vation was concluded by Lajeunesse et al. [2] where layers of coloured sand were used in the prepared column and the resultant deposit was split to reveal a conical zone where there had been no movement of material.

When entering the second geometric regime, the particulate above a height  $0.90r_0$  avalanches over the currently deposited matter and the height minutely continues to increase. It argued that this increase is marginally smaller for  $r_0 = 20, 25$  mm with exponents of 0.05 and 0.07 respectively, while for all other cylinder radii the relation

$$h_* = 0.90a^{0.09} \tag{10}$$

holds. In this case the meso-scale effect is observed for  $r_0/d \lesssim 40$ , likely to be arresting faster than the radial coefficient  $P_1$  due to the greater amount of material as presupposed for the radial coefficient  $P_2$ . Lajeunesse et al. suggest that there is no increase in height while Lube et al. agree that there is, although proposing a higher exponent of 0.17.

Mohr-Coulomb theory states that the development of surface failure is due to the inability to sustain its composition under shear stresses and occurs along an envelope projected at an angle equal to the internal friction angle  $\theta_\mu$ . The data provided for the limestone based particulate used indicated an internal friction angle  $\theta_\mu \approx 39^\circ$ . This would imply that the onset of the second geometric regime would occur at an aspect ratio of  $a = 0.89$  which is in good agreement with the experimental data. This allows description of the height with known material parameters:

$$\begin{aligned} h_* &= a & a < \tan \theta_\mu \\ h_* &= \tan(\theta_\mu)a^{0.09} & a > \tan \theta_\mu \end{aligned} \tag{11}$$

where 0.09 is exchanged for a lower value for the smallest  $r_0/d$ . Obtaining scalings where constants are completely

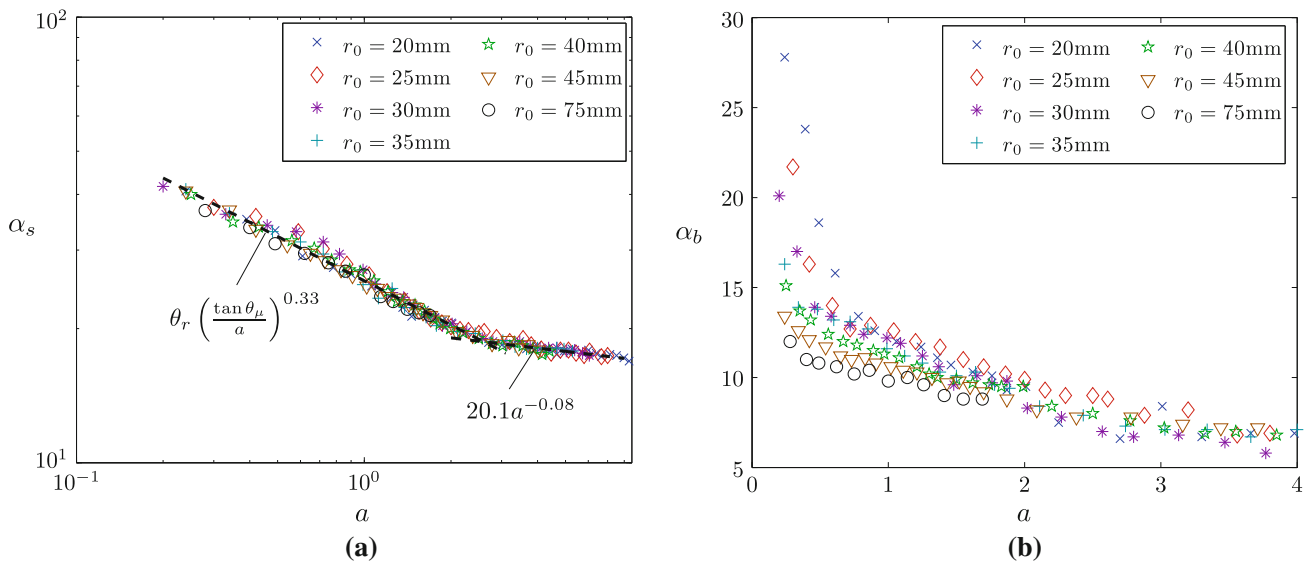


**Fig. 8** Variation in angle against aspect ratio for **a** summital angle, **b** base angle

described by the material parameters is desirable for equivalence in other experimental setups with different granular materials. This is an encouraging step to a fuller description of the final deposit independent of seemingly arbitrary proportional constants.

### 3.4 Angular profiling

The surface of the deposit does not have a straight edge as a cone does, but it curved to some angular profile. Two characteristic angles of the profile are the angle at the summit,  $\alpha_s$ , and the angle at the base,  $\alpha_b$ . These values were obtained from the 3D meshes generated, so the method was not intrusive or destructive of the deposit. Where the first geometric regime exists and there is a flat summit,  $\alpha_s$  was taken to be the angle of the slope directly below the flat surface.

For  $a \lesssim 3$  the summital angle was found to vary with aspect ratio as in Fig. 8a, following a power relation:

$$\alpha_s = 25.6a^{-0.33} \tag{12}$$

While the aspect ratio is such that the resulting deposit is a truncated cone, the avalanching periphery is strongly dependent upon the internal friction angle rather than the angle of repose as discussed in Sect. 3.3 and so  $\alpha_s > \theta_r$ . The onset of the second geometric regime where the entirety of the summit is consumed corresponds to the aspect ratio where material exists above the conical failure envelope defined by the internal friction angle. At aspect ratios greater than this critical onset, the greatest sustainable angle of a deposit with a sharp peak is exactly the angle of repose by definition. Hence where this occurs  $\alpha_s < \theta_r$ . The continued decrease in the summital angle is due to increased avalanching over already deposited layers smoothing the steep sides.

Using the angular analysis of the onset of the second geometric regime and assuming the summital angle to be a function of aspect ratio,  $\alpha_s(a)$ , we have the condition

$$\alpha_s(\tan \theta_\mu) = \theta_r \tag{13}$$

Applying this condition to Eq. (12) the coefficient can be expressed in terms of the internal parameters:

$$\alpha_s = \theta_r \left( \frac{\tan \theta_\mu}{a} \right)^{0.33} \tag{14}$$

Enabled by the previous analysis via interpretation of Mohr–Coulomb theory, this is the second scaling with constants given in terms of known material parameters.

When  $a \gtrsim 3$  a different relationship emerges coinciding with the change in collapse regime where the entire upper surface of the initial column falls retaining its horizontal profile. The angle at the summit continues to decrease but at a severely slower rate following the power law

$$\alpha_s = 20.1a^{-0.08} \tag{15}$$

The variation in the angle at the base with aspect ratio was found to be more complex and dependent upon the  $r_0$  and hence the initial system size as shown in Fig. 8b. While  $a \lesssim 3$  this follows a power law relation of the form

$$\alpha_b = Ea^{-F} \tag{16}$$

where  $E$  and  $F$  are constants dependent on  $r_0/d$  as given in Table 3. The dependence on  $r_0/d$  is initially linear up to  $r_0 = 45$  mm, giving relations

$$E = 14.7 - 0.066 \frac{r_0}{d} \tag{17}$$

$$F = 0.010 \frac{r_0}{d} - 0.78 \tag{18}$$



**Table 3** Constants fitting power law relation  $\alpha_b = Ea^{-F}$  for given initial cylinder size

$r_0$ (mm)	$r_0/d$	$E$	$F$
20	28	12.94	0.52
25	35	12.33	0.45
30	42	11.69	0.32
35	50	11.42	0.25
40	57	10.98	0.23
45	64	10.53	0.17
75	107	9.76	0.16

For  $r_0 = 75$  mm the  $F$  exponent evidently stagnates and it can be assumed that for  $r_0/d > 100$   $F = 0.16$ . With an error of  $\pm 1^\circ$  it is presupposed that  $E \approx 10$  for  $r_0/d > 100$ . For  $a \gtrsim 3$ ,  $\alpha_b$  stagnates with  $6^\circ < \alpha_b < 8^\circ$ .

For a fixed aspect ratio, smaller system sizes have a distinctly higher base angle at least in the first geometric regime. This would be expected given a proportionally smaller radius of the deposit and equivalently low  $r_0/d$  as described in Sect. 3.2. After the end of the first geometric regime the variation in angle between cylinder sizes becomes small and approaches the stagnation point. Within this range, avalanching of the upper surface of the column flows over the already deposited layers that stretch beyond 0.75 cylinder radii and are of similar thickness at the extremity.  $\alpha_b < \theta_r$  for all aspect ratios as expected or further avalanching would occur as per the definition of the angle of repose.

## 4 Conclusions

The methodology used in the experiments have allowed a substantially greater degree of accuracy than any previous research on the subject. Coupled with mesh generation of the deposits and the ability to obtain data non-intrusively, a deeper dependence on the scaling of granular collapse has been revealed. It was previously thought that in the absence of internal parameters, scalings of the collapse were uniquely describable in terms of the aspect ratio of the initial granular column. Given similar initial conditions to the previous studies, this analysis has shown that differences in data that were originally explained as experimental error are a demonstration of system size dependence calculated as  $r_0/d$ . While this dependence exists, it has demonstrated a saturation at the larger  $r_0/d$  with this particular point dependent on the scaling under consideration. Furthermore some relations are expressible in terms of internal parameters, desirable of all scalings for a full theoretical model of the collapse to exist.

It is well known that the final deposit radius has a linear dependence on aspect ratio, but results showed that the coefficient of this proportionality increased, at least initially,

with the system size. For values  $r_0/d \lesssim 70$  this proportionality was also linear, showing signs of abruptly saturating for  $r_0/d = 107$ . This behavior is mirrored in the angle at the base of the deposit; larger initial system sizes have a shallower base angle. Together these results support the idea that the initially deposited layers have an effect on the scalings of the resultant pile, with their deposition dependent upon the amount of initial mass collapse and the resultant jamming. For a fixed aspect ratio, a greater initial radius means a thicker initial deposit. The thicker deposit experiences greater jamming, and hence results in greater spreading of subsequently avalanching material and a shallower angle at the base of the resultant pile.

In the first geometric regime a summital plateau exists that shrinks with increasing aspect ratio. The continued contraction was directly proportional to aspect ratio, but had no relation to system size or rate of increase of the final pile radius. Within this first geometric regime the final height is exactly the initial height, but where  $a > \tan \theta_\mu$  the increase in height significantly slows of the order  $a^{0.09}$ . It is argued that the height increases even slower in the smaller systems with  $r_0/d = 28, 35$ . The angle at the summit follows a power law relation with aspect ratio, independent of system size, and coupled with other analysis is shown to depend on the angle of repose and internal friction while  $a \lesssim 1.7$ .

In summary, dimensions  $r_f$  and  $\alpha_b$  that result directly from material deposition depends strongly upon the initial system size  $r_0/d$  in addition to the aspect ratio and material parameters. Dimensions  $r_s$ ,  $h_f$  and  $\alpha_s$  which result from material loss to avalanching and not the history of the collapse have little or no secondary dependence and are subject only to aspect ratio and material parameters. This further fuels the necessity for any theoretical model of the collapse to incorporate internal dynamics such as those described by Cates et al. [13], particularly where investigations could contain a meso-scale effect.

**Acknowledgments** This research was funded by an EPSRC doctoral-training grant to whom we offer our gratitude.

## References

1. Lube, G., Huppert, H.E., Sparks, R.S.J., Hallworth, M.A.: Axisymmetric collapses of granular columns. *J. Fluid Mech.* **508**, 175–199 (2004)
2. Lajeunesse, E., Mangeney-Castelnau, A., Vilotte, J.P.: Spreading of a granular mass on a horizontal plane. *Phys. Fluids* **16**, 2371–2381 (2004)
3. Thompson, E.L., Huppert, H.E.: Granular column collapses: further experimental results. *J. Fluid. Mech* **575**, 177–186 (2007)
4. Staron, L., Hinch, E.J.: Study of the collapse of granular columns using two-dimensional discrete-grain simulation. *J. Fluid Mech.* **545**, 1–27 (2005)
5. Zenit, R.: Computer simulations of the collapse of a granular column. *Phys. Fluids* **17**, 031703 (2005)

6. Cleary, P.W., Frank, M.: Three-dimensional discrete element simulations of axi-symmetric collapses of granular columns. Technical Report 44710, Technische Universitat Kaiserslautern (2006)
7. Lacaze, L., Phillips, J.C., Kerswell, R.R.: Planar collapse of a granular column: experiments and discrete element simulations. *Phys. Fluids* **82**, 063302 (2008)
8. Tapia-McClung, H., Zenit, R.: Computer simulations of the collapse of columns formed by elongated grains. *Phys. Rev. E* **85**, 061304
9. Lube, G., Huppert, H.E., Sparks, R.S.J., Freundt, A.: Collapses of two-dimensional granular columns. *Phys. Rev. E* **72**, 041301 (2005)
10. Balmforth, N.J., Kerswell, R.R.: Granular collapse in two dimensions. *J. Fluid Mech.* **538**, 399–438 (2005)
11. Siavoshi, S., Kudrolli, A.: Failure of a granular step. *Phys. Rev. E* **71**, 051302 (2005)
12. Mangeney, A., Heinrich, P., Roche, R., Boudon, G., and Chemine, J.L.: Modeling of debris avalanche and generated water waves: application to real and potential events in montserrat. *Phys. Chem. Earth* **25**, 741–745 (2000)
13. Cates, M.E., Wittmer, J.P., Bouchad, J.P., Claudin, P.: Jamming, force chains and fragile matter. *Phys. Rev. Lett.* **81**, 1841–1844 (1998)
14. Savage, S.B., Hutter, K.: The motion of a finite mass of granular material down a rough incline. *J. Fluid. Mech.* **199**, 177–215 (1989)
15. Kadanoff, L.P.: Built upon sand: theoretical ideas inspired by granular flows. *Rev. Mod. Phys.* **71**, 435–443 (1999)
16. Douady, S., Andreotti, B., Daerr, A.: On granular surface flow equations. *Eur. Phys. J. B Cond. Matter* **11**, 131–142 (1999)
17. Haderer, K.P., Kuttler, C.: Dynamic models for granular matter. *Granul. Matter* **2**, 9–18 (1999)
18. Pouliquen, O., Forterre, Y.: Friction law for dense granular flows: application to the motion of a mass down a rough inclined plane. *J. Fluid Mech.* **453**, 133–151 (2002)
19. Larrieu, E., Staron, L., Hinch, E.J.: Raining into shallow water as a description of the collapse of a column of grains. *J. Fluid. Mech.* **554**, 259–270 (2006)
20. Doyle, E.E., Huppert, H.E., Lube, G., Made, H.M., and Sparkes, R.S.J.: Static and flowing regions in granular collapses down channels: Insight from a sedimenting shallow water model. *Phys. Fluids* **19**, 106601 (2007)
21. Crosta, G.B., Imposimato, S., Roddeman, D.: Numerical modelling of 2-d granular step collapse on erodible and nonerodible surface. *J. Geophys. Res.* **114**, 03020 (2009)
22. Lagr e, P.-Y., Staron, L., Popinet, S.: The granular column collapse as a continuum: validity of a two-dimensional Navier-Stokes model with a  $\mu(I)$ -rheology. *J. Fluid Mech.* **686**, 378–408 (2011)
23. ASME.: American Society of Mechanical Engineers: B89.4.22-2004 Methods for performance evaluation of articulated arm coordinate measuring machines (2004)
24. Kiraci, E., Attridge, A., Williams, M.A.: The use of laser scanning technology to improve the design process. *App. Mech. Mat.* **110**, 4118–4122 (2012)